Automatic Mandibular Semantic Segmentation of Teeth Pulp Cavity and Root Canals, and Inferior Alveolar Nerve on Pulpy3D Dataset

Mahmoud Gamal, Marwa Baraka, and Marwan Torki

Alexandria University, Alexandria, Egypt

Abstract. Accurate segmentation of the pulp cavity, root canals, and inferior alveolar nerve (IAN) in dental imaging is essential for effective orthodontic interventions. Despite the availability of numerous Cone Beam Computed Tomography (CBCT) scans annotated for individual dental-anatomical structures, there is a lack of a comprehensive dataset covering all necessary parts. As a result, existing deep learning models have encountered challenges due to the scarcity of comprehensive datasets encompassing all relevant anatomical structures.We present our novel Pulpy3D dataset, specifically curated to address dental-anatomical structures' segmentation and identification needs. Additionally, we noticed that many current deep learning methods in dental imaging prefer 2D segmentation, missing out on the benefits of 3D segmentation. Our study suggests a UNet-based approach capable of segmenting dental structures using 3D volume segmentation, providing a better understanding of spatial relationships and more precise dental anatomy representation. Pulpy3D contributed in creating the seeding model from 150 scans, which helped complete the remainder of the dataset. Other modifications in the architecture, such as using separate networks, one semantic network, and a multi-task network, were highlighted in the model description to show how versatile the Pulpy3D dataset is and how different models, architectures, and tasks can run on the dataset. Additionally, we stress the lack of attention to pulp segmentation tasks in existing studies, underlining the need for specialized methods in this area. The code and Pulpy3D links can be found at https://github.com/mahmoudgamal0/Pulpy3D

Keywords: Pulp Segmentation· Inferior Alveolar Nerve Segmentation · CBCT · UNet3D

1 Introduction and Related Work

With advancements in imaging technology, Cone Beam Computed Tomography (CBCT) has demonstrated significant improvements over traditional CT scans in the dental-maxillofacial area due to its ability to unveil the intricate details of small anatomical structures within the oral cavity. However, this ability remains underutilized due to the absence of comprehensive and task-specific datasets necessary for deep-learning models to perform various tasks, including tooth

and lesion detection, inferior alveolar nerve and bone segmentation, and pulp cavity and root segmentation.

Navigating the pulp and root morphology variations among different individuals and age groups presents a tough challenge. Current methodologies [5, 17] typically approach this challenge by initially isolating the hard tooth structure, then extracting the pulp region and proceeding with segmentation. However, many existing solutions rely on 2D slices [19], neglecting the volumetric features inherent in 3D volumes.

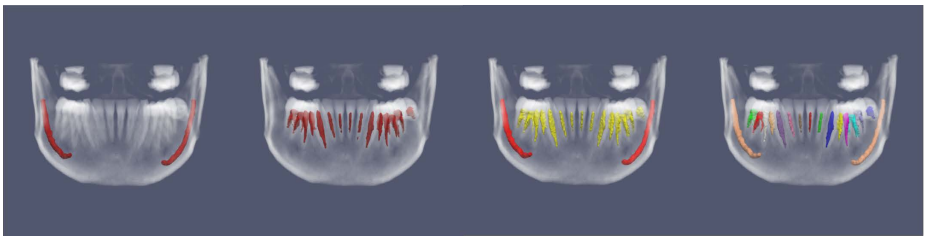

Fig. 1. Example 3D CBCT scan with overlaid annotations. Left: IAN annotation from ToothFairy. Left Center: Pulp annotation from Pulpy3D. Right Center: Pulp and IAN annotations from Pulpy3D. Right: Instance annotations of pulp and IAN from Pulpy3D.

Accurately segmenting the Inferior Alveolar Nerve (IAN) is crucial in surgeries involving dental implant placement in the jawbone, where precision is paramount due to the proximity of the IAN. Segmenting the dental pulp and root canal morphology is crucial for successful root canal treatments and reducing failures and retreatment cases. Utilizing 3D pulp segmentations and reconstructed surface models aids in accurately rebuilding anatomical structures, enhancing treatment outcomes. Comprehending internal anatomy relationships is vital before proceeding with endodontic therapy, enabling a precise diagnosis. Figure 1 shows an example of pulp cavity, root, and IAN.

In this paper, we introduce the Pulpy3D dataset based on 3D CBCT scans. Pulpy3D is the largest publicly available dataset for both pulp and IAN segmentation. This is a unique contribution to the community, which we believe will bring more attention to the problem of pulp segmentation and will allow the rise of more literature on both dental research and deep learning algorithms. Also, we provided comparisons of three approaches to solving the segmentation problem(s) based on single and multi-task semantic segmentation objectives. We also propose the APPU model, which is based on the POSPADUNET [3] by adding gated attention blocks, which proved to be a better choice for our experiments.

1.1 Related Work

In this section, we discuss the most relevant work on the segmentation of mandibular structures, specifically focusing on teeth pulp cavity, root canals, and (IAN).

Non-Deep Learning Methods: Active contour models have been utilized in tooth segmentation from volumetric CT images by employing a 2D level set method on a slice-by-slice basis [7, 21]. Contour propagation through consecutive 2D slices from CT scans allows a better view of the reconstructed 3D volume when all the 2D slices were concatenated [6]. A hybrid level-set and mesh segmentation technique [18] involved the use of CT scans, where both maxillary and mandible teeth were in contact. As CBCT scans became more common, the optimal segmentation threshold was achieved by employing an algorithm that uses the plane intercept histogram of reciprocal cross entropy which is followed by the binarization technique [16].

Pulp Cavity Segmentation: Pulp cavity and root segmentation were achieved by a long-short residual connection encoder-decoder network. The output masks were then processed by an advanced level set algorithm called 3D Chan-Vese [23]. CBCT scans combined with panoramic views were utilized to extract bounding boxes for single-rooted and multi-rooted teeth using an RPN with an FPN backbone. These bounding boxes were subsequently fed into a UNet to refine pulp segmentation [5]. 2D CBCT slices were fed into a 2D UNet and MWT for the segmentation of jaw, teeth, and pulp chambers [19]. To prioritize root segmentation, multitask approaches involving tooth and pulp segmentation were employed. In the first stage, DentalNet extracted feature maps for tooth instance segmentation and identification. In the second stage, ROI extraction and PulpNet performed pulp segmentation and ROI refinement using regression heat maps [17].

IAN Segmentation: Deep label propagation and positional embeddings of volumetric CBCT voxels showed significant improvements in IAN segmentation [3]. Through the process of selective retraining, a semi-supervised self-training nnUNet with Strong data augmentation produced better results [11]. IAN segmentation is not only applicable to CBCT scans. Efficient UNet models produced IAN segmentation on panoramic scans of the maxillofacial area [20].

2 Pulpy3D Dataset

2.1 Motivation

Most of the previous studies were done on 2D slices of 3D CBCT scans or presented insufficient 3D CBCT scans due to a lack of labeled samples in the literature [3, 24]. Few studies were done on voxels of single teeth cut from the complete CBCT scan [5, 7, 10, 17]. Other studies had less than 100 samples for the whole study [1, 9, 16, 15, 24]. These factors motivated us to introduce Pulpy3D which is the largest publicly available 3D CBCT dataset that provides the annotations for the pulp and IAN in the same scans. We based our new dataset on the ToothFairy [2] dataset which provided the IAN segmentation annotations only.

2.2 Description

Pulpy3D[1] consists of the original 443 scans of the lower mandibular jaw of the ToothFairy Dataset[2] [2]. Each scan file is associated with five ground truth annotations. In addition to the annotations for IAN segmentation labels from the ToothFairy dataset, we provide the pulp segmentation labels, pulp instance segmentation labels, and the combined labels for merging the pulp with IAN. Our dataset contains the splits used to define the train set, test set, and validation set. We accompany the dataset with the definition of labels and label maps of the teeth according to the FDI teeth numbering system.

2.3 Data Collection

Considering the pulp annotations, we used 150 random scans from the Tooth-Fairy dataset. Dental medical experts and practitioners, led by an individual with 15 years of experience, manually annotated the pulp cavity and root canals using the ITK-Snap tool [22]. We then used our pre-trained model, discussed later, to learn how to segment the pulp space. We used the model weights to infer the remaining (293) scans. Dental experts performed minor fixes while reviewing the model outputs. We have also provided annotations of the mandibular jaw only after we cut the maxillary parts.

Instance segmentation annotated labels of each single tooth pulp in the mandibular jaw were created and included in Pulpy3D. The class label would be the number of the tooth according to the FDI numbering system. Instance labels were obtained by performing the clustering algorithm DBSCAN [4] on the generated semantic segmentation labels. Then, using a hybrid approach that involves manual intervention and automation tools that we developed, we were able to perform one-click relabeling of the clusters obtained from DBSCAN.

Nerve annotations are obtained from the original ToothFairy dataset [2]. All CBCT scans contain sparse labels which are very small indications of where the nerve should be. The sparse labels are easier to create manually. These labels undergo circular expansion [3] to be able to train our model.

3 Model Description

Our model architecture is based on POSPADUNET [3] which was used for the segmentation of the inferior alveolar nerve. We extended this setting to make our network, Attention-POSPADUNET (APPU), which was equipped with gated attention blocks [13]. Figure 2 shows the architecture for the APPU. We propose different benchmarks on the Pulpy3D dataset using various architectures. The architectures explore separate independent networks for segmenting the pulp and IAN. We also discuss multi-task segmentation using a single semantic network and two decoder networks.

[1] Pulpy3D will be available publicly upon the acceptance of the paper.
[2] The training set, named ToothFairy Dataset, is publicly available under CC BY-SA.

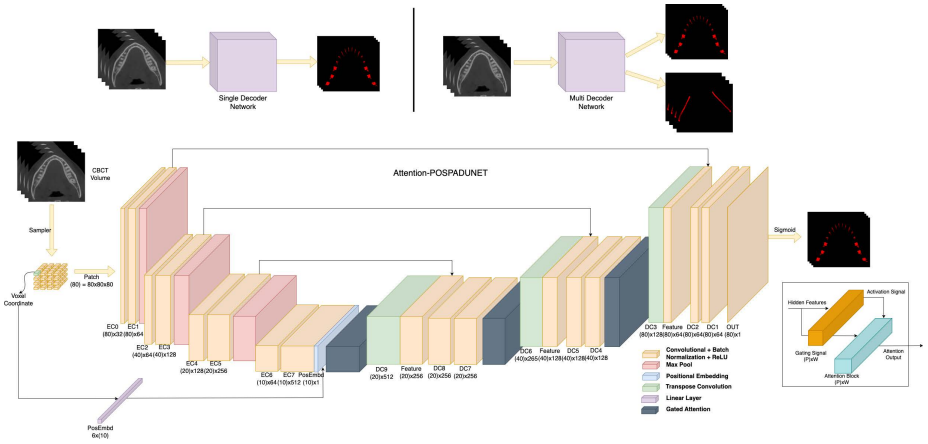

Fig. 2. Top Left: Single Encoder-Decoder organization based on APPU. Top Right: Multi-task organization based on APPU. Bottom: Detailed breakdown of encoder and decoder architectures. Best seen in zoom and color

3.1 Single Task

We employed the APPU model in a single-mode semantic segmentation task, training a single instance of the model for a specific purpose.

Two Separate Nets Two distinct APPU models were used: one dedicated to segmenting pulp and root structures, and another focused on the IAN. The predictions generated by both models were then combined into a unified prediction.

One Semantic Network An alternative approach involved training a single APPU model capable of predicting segmentations for both the pulp and IAN with distinct labels (see Figure 1).

3.2 Multi-task

We perform a multi-task training approach [1, 17] in which the contracting path is used as a commonly shared encoder and the expanding path is used as a decoder. We use two decoders, one for the pulp cavity and root canal segmentation and the other for the IAN segmentation. Figure 2 shows the used network architectures.

4 Experiments and Results

In this section, we discuss the experiments carried on with the Pulpy3D dataset and the results achieved.

4.1 Implementation Details

All experiments were run using Python 3.10.12 and PyTorch 2.0.1 on Nvidia RTX 4090 24GB GPU. We used TorchIO 0.19.1 for image preprocessing and sampling using Label Sampler. Stochastic Gradient Descent (SGD) was chosen as the optimizer with a starting learning rate of 0.1 and a plateau multi-step learning rate. Our main metrics are mean Dice Similarity Coefficient (DSC) and mean Intersection over Union (IoU). A single experiment for such models would take approximately two to three days in this setting.

Table 1. Baseline Comparison for Seeding Model

Model	DSC	IoU
POSPADUNET[3]	0.76018	0.6159
UNETR[8]	0.73018	0.5777
UNET3D[14]	0.55529	0.3867
VNET3D[12]	0.63134	0.4655
APPU	**0.76693**	**0.6242**

4.2 Quantitative Evaluation

Seeding Model Selection Manually annotating the 3D CBCT for pulp segmentation is overly labor-intensive. We recognized that developing a seeding model would significantly reduce the time required to annotate the original 443 3D CBCT scans from ToothFairy. We accelerated the annotation process by evaluating various baselines on 150 scans, with 17 reserved for testing purposes. The subsequent step involves generating candidate segmentation masks using the most effective seeding model and enabling dental experts to review and refine the segmentation masks. Notably, annotating the initial 150 scans without the seeding model took approximately 8 hours per scan. However, with the seeding model, dental experts reviewed and edited the masks within just half an hour per scan.

Another benefit obtained from the seeding model was a reduction in the training time required for our subsequent experiments. This was achieved by evaluating multiple baselines on the limited set of 150 scans and later selecting the best-performing model for all future experiments. Table 1 illustrates that basic UNET3D and VNET3D did not perform well. UNETR, a transformer-based UNET, outperformed UNET3D and VNET3D. However, a significant enhancement was observed with the utilization of Positional Padding UNET (POSPADUNET) compared to other baselines.

A third advantage is introducing our APPU model, as detailed in Section 3. We leverage the attention mechanism and the superiority of POSPADUNET compared to other baselines. From Table 1, we note a slight improvement in the Dice Similarity Coefficient and a more substantial increase in the Intersection over Union.

Segmentation Results We ran multiple experiments: a single-task network for pulp segmentation, a single-task network for nerve segmentation, a single-task semantic segmentation network for pulp and nerve collectively, and a multi-task network for pulp and nerve. We used 373 scans for training, 30 for validation, and 40 for testing. Table 2 presents the scores obtained for the segmentation tasks.

We observe that the best-performing approach is to have two separate networks, one for pulp segmentation and the second for the IAN segmentation. The multi-task with one encoder and two decoders performed the worst since the IAN structure differs from the pulp.

We observe that the semantic segmentation network did a better job for the joint pulp and IAN segmentation task when compared to the multi-task approach. However, we can see that the multi-task approach did better for IAN segmentation.

Table 2. Segmentation results of training two networks separately. Bold values indicate the best result. Underlined values indicate the second-best result.

Output	DSS	IoU
Unified Segmentation from two separate networks		
Pulp Segmentation	**0.7958**	**0.7019**
IAN Segmentation	**0.7543**	**0.6183**
Pulp + IAN Segmentation	**0.7820**	**0.6524**
Semantic Segmentation of a single network		
Pulp Segmentation	<u>0.7589</u>	<u>0.6530</u>
IAN Segmentation	0.7015	0.5520
Pulp + IAN Segmentation	<u>0.7383</u>	<u>0.5958</u>
Multi-task common encoder multiple decoders network		
Pulp Segmentation	0.7362	0.6213
IAN Segmentation	<u>0.7201</u>	<u>0.5761</u>
Pulp + IAN Segmentation	0.7252	0.5803

4.3 Qualitative Evaluation

We present visual representations of predicted labels compared to ground truth labels. Figure 3 displays predicted labels for one patient, illustrating how the labels manifest across three planes. Additionally, Figure 4 presents a 3D visualization comparing the ground truth labels with the predicted ones, highlighting the disparities between them[3].

For the two single networks, we observe some islands mainly in the nerve segmentation, which can be further removed by applying a post-processing scheme.

[3] Codes and results will be available on GitHub after acceptance.

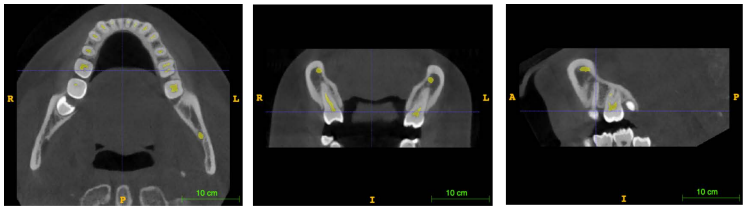

Fig. 3. Predicted pulp and nerve labels, left: axial, center: coronal, right: sagittal

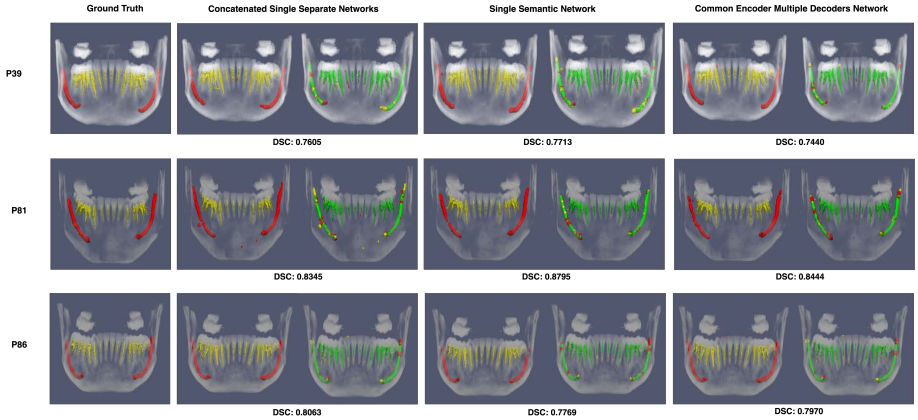

Fig. 4. Example results from 3D segmentation of pulp and nerve. Ground truth labels are leftmost. Each pair has prediction labels, left, and overlapping of ground truth labels with predictions, right. The overlapping of labels has the following color code: Green for True Positives, Yellow for False Positives, and Red for False Negatives.

5 Conclusion and Future Work

In conclusion, the present study has provided valuable contributions to developing an automatic pipeline for mandibular semantic segmentation, demonstrating promising results for segmenting teeth pulp cavity, root canals, and the Inferior Alveolar Nerve (IAN) on 3D CBCT scans. Henceforth, this endeavor opens up various opportunities for future research and enhancements. For example, instance segmentation to uniquely identify each tooth number is a promising direction. Additionally, augmenting the Pulpy3D dataset with supplementary labels for tooth-hard tissue could enhance segmentation accuracy. Furthermore, incorporating different annotations to identify lesions, cavities, and other dental anomalies holds the potential for constructing a complete segmentation scheme.

Disclosure of Interests. The authors have no competing interests to declare that are relevant to the content of this article.

References

1. Chen, Y., Du, H., Yun, Z., Yang, S., Dai, Z., Zhong, L., Feng, Q., Yang, W.: Automatic segmentation of individual tooth in dental cbct images from tooth surface map by a multi-task fcn. IEEE Access **8**, 97296–97309 (2020). https://doi.org/10.1109/ACCESS.2020.2991799
2. Cipriano, M., Allegretti, S., Bolelli, F., Di Bartolomeo, M., Pollastri, F., Pellacani, A., Minafra, P., Anesi, A., Grana, C.: Deep segmentation of the mandibular canal: a new 3d annotated dataset of cbct volumes. IEEE Access **10**, 11500–11510 (2022). https://doi.org/10.1109/ACCESS.2022.3144840
3. Cipriano, M., Allegretti, S., Bolelli, F., Pollastri, F., Grana, C.: Improving segmentation of the inferior alveolar nerve through deep label propagation (2022), https://ditto.ing.unimore.it/maxillo/
4. Deng, D.: Dbscan clustering algorithm based on density. pp. 949–953. Institute of Electrical and Electronics Engineers Inc. (9 2020). https://doi.org/10.1109/IFEEA51475.2020.00199
5. Duan, W., Chen, Y., Zhang, Q., Lin, X., Yang, X.: Refined tooth and pulp segmentation using u-net in cbct image. Dentomaxillofacial Radiology **50** (9 2021). https://doi.org/10.1259/dmfr.20200251
6. Gan, Y., Xia, Z., Xiong, J., Zhao, Q., Hu, Y., Zhang, J.: Toward accurate tooth segmentation from computed tomography images using a hybrid level set model. Medical Physics **42**, 14–27 (1 2015). https://doi.org/10.1118/1.4901521
7. Gao, H., Chae, O.: Individual tooth segmentation from ct images using level set method with shape and intensity prior. Pattern Recognition **43**, 2406–2417 (7 2010). https://doi.org/10.1016/j.patcog.2010.01.010
8. Hatamizadeh, A., Tang, Y., Nath, V., Yang, D., Myronenko, A., Landman, B., Roth, H., Xu, D.: Unetr: Transformers for 3d medical image segmentation (3 2021), http://arxiv.org/abs/2103.10504
9. Lee, J., Chung, M., Lee, M., Shin, Y.G.: Tooth instance segmentation from cone-beam ct images through point-based detection and gaussian disentanglement (2 2021), http://arxiv.org/abs/2102.01315
10. Lin, X., Fu, Y., Ren, G., Yang, X., Duan, W., Chen, Y., Zhang, Q.: Micro–computed tomography–guided artificial intelligence for pulp cavity and tooth segmentation on cone-beam computed tomography. Journal of Endodontics **47**, 1933–1941 (12 2021). https://doi.org/10.1016/j.joen.2021.09.001
11. Liu, Y., Xin, R., Yang, T., Wang, L.: Inferior alveolar nerve segmentation in cbct images using connectivity-based selective re-training (8 2023), http://arxiv.org/abs/2308.09298
12. Milletari, F., Navab, N., Ahmadi, S.A.: V-net: Fully convolutional neural networks for volumetric medical image segmentation (6 2016), http://arxiv.org/abs/1606.04797
13. Oktay, O., Schlemper, J., Folgoc, L.L., Lee, M., Heinrich, M., Misawa, K., Mori, K., McDonagh, S., Hammerla, N.Y., Kainz, B., Glocker, B., Rueckert, D.: Attention u-net: Learning where to look for the pancreas (4 2018), http://arxiv.org/abs/1804.03999
14. Ronneberger, O., Fischer, P., Brox, T.: U-net: Convolutional networks for biomedical image segmentation (5 2015), http://arxiv.org/abs/1505.04597
15. Wang, H., Minnema, J., Batenburg, K.J., Forouzanfar, T., Hu, F.J., Wu, G.: Multiclass cbct image segmentation for orthodontics with deep learning. Journal of Dental Research **100**, 943–949 (8 2021). https://doi.org/10.1177/00220345211005338

16. Wang, L., peng Li, J., pu Ge, Z., Li, G.: Cbct image based segmentation method for tooth pulp cavity region extraction. Dentomaxillofacial Radiology **48** (2019). https://doi.org/10.1259/dmfr.20180236
17. Wang, Y., Xia, W., Yan, Z., Zhao, L., Bian, X., Liu, C., Qi, Z., Zhang, S., Tang, Z.: Root canal treatment planning by automatic tooth and root canal segmentation in dental cbct with deep multi-task feature learning. Medical Image Analysis **85** (4 2023). https://doi.org/10.1016/j.media.2023.102750
18. Xia, Z., Gan, Y., Chang, L., Xiong, J., Zhao, Q.: Individual tooth segmentation from ct images scanned with contacts of maxillary and mandible teeth. Computer Methods and Programs in Biomedicine **138**, 1–12 (1 2017). https://doi.org/10.1016/j.cmpb.2016.10.002
19. Yang, H., Wang, X., Li, G., Yang, H..: Tooth and pulp chamber automatic segmentation with artificial intelligence network and morphometry method in cone-beam ct segmentación automática de cámaras dentales y pulpares con red de inteligencia artificial y método de morfometría en tc de haz cónico (2022)
20. Yang, S., Li, A., Li, P., Yun, Z., Lin, G., Cheng, J., Xu, S., Qiu, B.: Automatic segmentation of inferior alveolar canal with ambiguity classification in panoramic images using deep learning. Heliyon **9** (2 2023). https://doi.org/10.1016/j.heliyon.2023.e13694
21. Yau, H.T., Yang, T.J., Chen, Y.C.: Tooth model reconstruction based upon data fusion for orthodontic treatment simulation. Computers in Biology and Medicine **48**, 8–16 (5 2014). https://doi.org/10.1016/j.compbiomed.2014.02.001
22. Yushkevich, P.A., Piven, J., Cody Hazlett, H., Gimpel Smith, R., Ho, S., Gee, J.C., Gerig, G.: User-guided 3D active contour segmentation of anatomical structures: Significantly improved efficiency and reliability. Neuroimage **31**(3), 1116–1128 (2006)
23. Zheng, Q., Ge, Z., Du, H., Li, G.: Age estimation based on 3d pulp chamber segmentation of first molars from cone-beam-computed tomography by integrated deep learning and level set (2021). https://doi.org/10.1007/s00414-020, https://doi.org/10.1007/s00414-020-
24. Zheng, Z., Yan, H., Setzer, F.C., Shi, K.J., Mupparapu, M., Li, J.: Anatomically constrained deep learning for automating dental cbct segmentation and lesion detection. IEEE Transactions on Automation Science and Engineering **18**, 603–614 (4 2021). https://doi.org/10.1109/TASE.2020.3025871